Inorganic Chemistry

Article

pubs.acs.org/IC

Noncentrosymmetric $YVSe_2O_8$ and Centrosymmetric $YVTe_2O_8$: Macroscopic Centricities Influenced by the Size of Lone Pair Cation Linkers

Yeong Hun Kim, Dong Woo Lee, and Kang Min Ok*

Department of Chemistry, Chung-Ang University, 221 Heukseok-dong, Dongjak-gu, Seoul 156-756, Republic of Korea

Supporting Information

ABSTRACT: Two new quaternary vanadium selenite and tellurite, i.e., $YVSe_2O_8$ and $YVTe_2O_8$, have been synthesized through hydrothermal and solid-state reactions. Both of the reported materials exhibit three-dimensional framework structures that are composed of layers of corner-shared VO_6 octahedra, layers of edge-shared YO_8 groups, and SeO_3 or TeO_3 linkers. While $YVSe_2O_8$ crystallizes in the orthorhombic noncentrosymmetric (NCS) space group, *Abm*2, $YVTe_2O_8$ reveals the monoclinic centrosymmetric (CS) space group, *C*2/*m*. The band gaps for $YVSe_2O_8$ and $YVTe_2O_8$ are calculated to be 2.7 and 2.2 eV, respectively, from the UV−vis diffuse reflectance spectra. Powder second harmonic generation (SHG) measurements using 1064 nm radiation reveals that NCS $YVSe_2O_8$ has a similar SHG efficiency to that of $NH_4H_2PO_4$ (ADP). Detailed explanations of the structure−property relationships, effect of lone pair cation size on the macroscopic centricities, and full characterizations including infrared spectroscopy, thermal analyses, and elemental analyses are also presented.

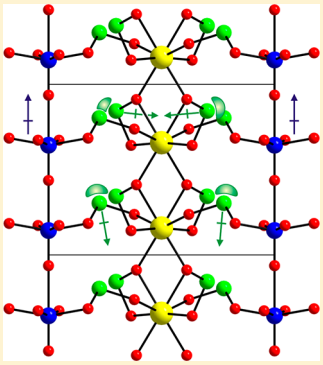

INTRODUCTION

Exploring new noncentrosymmetric (NCS) materials is an ongoing challenge because of their extremely important characteristics such as second-order nonlinear optical (NLO), piezoelectric, ferroelectric, and pyroelectric properties.[1] Thus, a variety of efforts have been made to discover functional NCS materials by combining cations with asymmetric environments as building blocks. Macroscopic NCS structures in oxide materials with extended structures are often found in two families of cations, namely, d^0 transition metal cations with octahedral coordination moieties (V^{5+}, Mo^{6+}, W^{6+}, etc.) and lone pair cations (Sb^{3+}, Se^{4+}, Te^{4+}, etc.). Both families of cations tend to exhibit distortive coordination environments attributable to the second-order Jahn−Teller (SOJT) effects.[2] With d^0 transition metal cations in octahedral coordination environments, the SOJT effects generally occur when the empty metal d-orbitals mix with the filled ligand p-orbitals. The octahedral distortions are normally observed from the center toward an edge (local C_2 direction), toward a face (local C_3 direction), or toward a corner (local C_4 direction).[3] With the lone pair cations, however, the strong interaction of the s- and p-orbitals of cation with the anion p-orbitals is crucial for lone pair formation and the subsequent cationic distortion.[4] Other important cationic families of NCS chromophores are d^{10} transition metal cations and borate groups with asymmetric π-orbital systems.[5] It is now getting more important to understand factors determining the overall centricity: the above-mentioned local asymmetric units normally align in antiparallel manner and result in crystallographic centrosymmetric (CS) structures, unless the specific situations influencing the space group symmetry are rationally controlled. A few important factors that can help to determine the macroscopic centricity are the size of metal cations, the hydrogen-bonding effects, and the framework flexibility.[6] While we investigated the Y^{3+}−V^{5+}−Q^{4+} (Q = Se or Te)−oxide system, we discovered two new stoichiometrically similar quaternary vanadium selenite and tellurite. Thus far, several stoichiometrically similar quaternary vanadium selenites or tellurites materials, i.e., $M^{3+}VQ_2O_8$ (M = Bi, Eu, Gd, Tb, In, and Sc), have been reported.[7] Herein we report synthesis, structure determination, second-harmonic generation (SHG) properties, and characterization of two new mixed vanadium oxides, $YVSe_2O_8$ and $YVTe_2O_8$. The effect of lone pair cation size on the macroscopic centricities will also be discussed.

EXPERIMENTAL SECTION

Reagents. Y_2O_3 (Alfa Aesar, 99.9%), V_2O_5 (Junsei, 99%), SeO_2 (Aldrich, 99.8%), and TeO_2 (Alfa Aesar, 98%) were used as received.

Synthesis. Single crystals of $YVSe_2O_8$ were grown through a hydrothermal reaction. A 0.113 g portion (5.00×10^{-4} mol) of Y_2O_3, 0.091 g (5.00×10^{-4} mol) of V_2O_5, 0.222 g (2.00×10^{-3} mol) of SeO_2, and 5 mL of deionized water were placed in a 23 mL of Teflon-lined stainless steel autoclave. The reactor was tightly sealed and heated to 230 °C for 4 days, and cooled to room temperature at a rate of 6 °C h^{-1}. After cooling, the autoclave was opened, and the products were recovered by filtration and washed with distilled water. The products contained light green crystals of $YVSe_2O_8$ and colorless crystals of $Y(SeO_3)(HSeO_3)\cdot 2H_2O$,[8] which was confirmed by single-crystal X-ray diffraction. Crystals of $YVTe_2O_8$ were obtained by a standard solid-state reaction. A 0.113 g portion (5.00×10^{-4} mol) of Y_2O_3, 0.091 g (5.00×10^{-4} mol) of V_2O_5, and 0.638 g (4.00×10^{-3}

Received: November 26, 2013
Published: January 2, 2014

   dx.doi.org/10.1021/ic402929m | Inorg. Chem. 2014, 53, 1250−1256

mol) of TeO_2 were ground thoroughly using an agate mortar and a pestle, and then pressed into a pellet. The pellet was transferred into a fused silica tube. The tube was evacuated for 20 min and flame-sealed. The sealed silica tube was heated to 650 °C for 48 h and cooled to 500 °C at a rate of 3 °C h^{-1} before being quenched to room temperature. Yellow crystals of $YVTe_2O_8$ were grown with some amorphous phases from the reaction.

Pure polycrystalline samples of $YVSe_2O_8$ and $YVTe_2O_8$ were synthesized by similar solid-state reactions. Stoichiometric amounts of Y_2O_3, V_2O_5, and SeO_2 (or TeO_2) were thoroughly mixed and pressed into pellets. The pellets were introduced into quartz tubes that were evacuated and sealed. The tubes were heated to 450 °C for $YVSe_2O_8$ and 550 °C for $YVTe_2O_8$ for 48 h with three intermediate regrindings. The powder X-ray diffraction data on the obtained bulk samples revealed that each synthesized material was pure and was in very good agreement with the calculated patterns from the single-crystal data (see the Supporting Information).

Single Crystal X-ray Diffraction. The structures of $YVSe_2O_8$ and $YVTe_2O_8$ were solved and refined by standard crystallographic methods. A green block (0.017 × 0.020 × 0.032 mm^3) for $YVSe_2O_8$ and a light yellow block (0.021 × 0.025 × 0.041 mm^3) for $YVTe_2O_8$ were used for single crystal data analyses. Diffraction data were collected at room temperatures using a Bruker SMART BREEZE diffractometer equipped with a CCD area detector using graphite monochromated Mo Kα radiation. To collect a hemisphere of data, a narrow-frame method was used with an exposure time of 10 s/frame, and scan widths of 0.30° in ω. The first 50 frames were remeasured at the end of the data collection in order to monitor instrument and crystal stability. The maximum correction applied to the intensities was <1%. The data were integrated using the SAINT program,[9] with the intensities corrected for polarization, Lorentz factor, air absorption, and absorption attributed to the variation in the path length through the detector faceplate. ψ scans were applied for the absorption correction on the hemisphere of data. The data were solved with SHELXS-97[10] and refined using SHELXL-97.[11] The orthorhombic metrics observed in $YVTe_2O_8$ suggest pseudomerohedral twinning of the crystal from Laue class 2/m to mmm. In fact, when we refined the structure in the orthorhombic space group, $Cmca$, all the constituent atoms were disordered, and unreasonable coordination environments occurred. The structure for $YVTe_2O_8$, however, was successfully refined in the monoclinic space group, $C2/m$. All crystallographic calculations were performed using the WinGX-98 software package.[12] Crystallographic data and selected bond distances for the reported materials are summarized in Tables 1 and 2, respectively.

Powder X-ray Diffraction. Powder X-ray diffraction was used to ensure the phase purities for the synthesized materials. The powder XRD data were collected on a Bruker D8-Advance diffractometer using Cu Kα radiation at room temperature with 40 kV and 40 mA in the 2θ range 5–70°. The experimental powder XRD patterns for the reported materials are in very good agreement with those calculated data from the single-crystal models.

Infrared Spectroscopy. Infrared spectra for $YVSe_2O_8$ and $YVTe_2O_8$ were recorded on a Varian 1000 FT-IR spectrometer in the 400–4000 cm^{-1} range, with the sample contained in a KBr matrix.

UV–Vis Diffuse Reflectance Spectroscopy. UV–vis diffuse reflectance data were collected on a Varian Cary 500 scan UV–vis–NIR spectrophotometer over the spectral range 200–2500 nm at room temperature at the Korea Photonics Technology Institute. Reflectance spectra were transformed to the absorbance using the Kubelka–Munk function.[13]

Thermogravimetric Analysis. Thermogravimetric analysis was carried out on a Setaram LABSYS TG-DTA/DSC thermogravimetric analyzer. The polycrystalline samples of $YVSe_2O_8$ and $YVTe_2O_8$ were contained within alumina crucibles and heated from room temperature to 1000 °C at a rate of 10 °C min^{-1} under flowing argon.

Scanning Electron Microscopy/Energy Dispersive Analysis by X-ray (SEM/EDAX). SEM/EDAX has been carried out using a Hitachi S-3400N and a Horiba Energy EX-250 instrument. EDAX for $YVSe_2O_8$ and $YVTe_2O_8$ exhibit Y:V:Se (or Te) ratios of 1.1:1.0:2.1 and 0.8:1.0:2.0, respectively.

Second-Order Nonlinear Optical Measurements. $YVSe_2O_8$ crystallized in a NCS space group $Abm2$; thus, SHG measurements on polycrystalline samples were performed through a modified Kurtz-NLO measurement system[14] using 1064 nm radiation. A Q-switched Nd:YAG laser (DAWA), that is operating at 20 Hz, was used for the measurements. Because powder SHG efficiency has been shown to strongly depend on particle size, polycrystalline samples were further ground and sieved (Newark Wire Cloth Co.) into individual particle size ranges (20–45, 45–63, 63–75, 75–90, 90–125, 125–150, 150–200, 200–250, >250 μm). Powder samples with particle size ranging 45–63 μm were used for comparing SHG intensities. All the samples with different particle sizes were put in separate capillary tubes. No index matching fluid was employed in any of the experiments. The SHG light, i.e., 532 nm light, was gathered in reflection and detected by a Hamamatsu photomultiplier tube. A 532 nm narrow-pass interference filter was attached to the tube to detect only the SHG light. To monitor the SHG signal, a digital oscilloscope (Tektronix

Table 1. Crystallographic Data for $YVSe_2O_8$ and $YVTe_2O_8$

	$YVSe_2O_8$	$YVTe_2O_8$
fw	425.77	523.05
space group	$Abm2$ (No. 39)	$C2/m$ (No. 12)
a (Å)	10.4036(4)	7.9396(10)
b (Å)	7.5904(3)	7.5625(10)
c (Å)	7.8341(3)	21.282(2)
β (deg)	90	90.010(10)
V (Å^3)	618.64(4)	1277.85(3)
Z	4	8
T (K)	298.0(2)	298.0(2)
λ (Å)	0.710 73	0.710 73
ρ_{calcd} (g cm^{-3})	4.571	5.438
μ (mm^{-1})	22.617	19.458
Flack parameter	−0.06(3)	N/A
$R(F)^a$	0.0463	0.0288
$R_w(F_o^2)^b$	0.1126	0.0682

$^aR(F) = \Sigma||F_o| - |F_c||/\Sigma|F_o|$. $^bR_w(F_o^2) = [\Sigma w(F_o^2 - F_c^2)^2/\Sigma w(F_o^2)^2]^{1/2}$.

Table 2. Selected Bond Distances (Å) for $YVSe_2O_8$ and $YVTe_2O_8$

$YVSe_2O_8$		$YVTe_2O_8$	
V(1)–O(1) × 2	1.923(9)	V(1)–O(4)	1.911(4)
V(1)–O(2)	1.616(4)	V(1)–O(6)	1.909(4)
V(1)–O(2)	2.301(14)	V(1)–O(9)	1.950(2)
V(1)–O(3) × 2	1.972(4)	V(1)–O(10)	1.628(4)
Se(1)–O(1) × 2	1.722(8)	V(1)–O(10)	2.342(4)
Se(1)–O(4)	1.690(12)	V(1)–O(11)	1.953(2)
Se(2)–O(5)	1.724(12)	Te(1)–O(1) × 2	1.879(4)
Se(2)–O(6) × 2	1.703(8)	Te(1)–O(2)	1.893(5)
Y(1)–O(4) × 2	2.360(7)	Te(2)–O(3)	1.858(5)
Y(1)–O(5) × 2	2.365(7)	Te(2)–O(4) × 2	1.906(4)
Y(1)–O(6) × 2	2.326(9)	Te(3)–O(5)	1.846(5)
Y(1)–O(6) × 2	2.369(9)	Te(3)–O(6) × 2	1.912(4)
		Te(4)–O(7) × 2	1.878(4)
		Te(4)–O(8)	1.891(5)
		Y(1)–O(1) × 2	2.331(4)
		Y(1)–O(1) × 2	2.439(4)
		Y(1)–O(2) × 2	2.393(3)
		Y(1)–O(3) × 2	2.304(3)
		Y(2)–O(5) × 2	2.312(3)
		Y(2)–O(7) × 2	2.336(4)
		Y(2)–O(7) × 2	2.436(4)
		Y(2)–O(8) × 2	2.391(3)

dx.doi.org/10.1021/ic402929m | Inorg. Chem. 2014, 53, 1250–1256

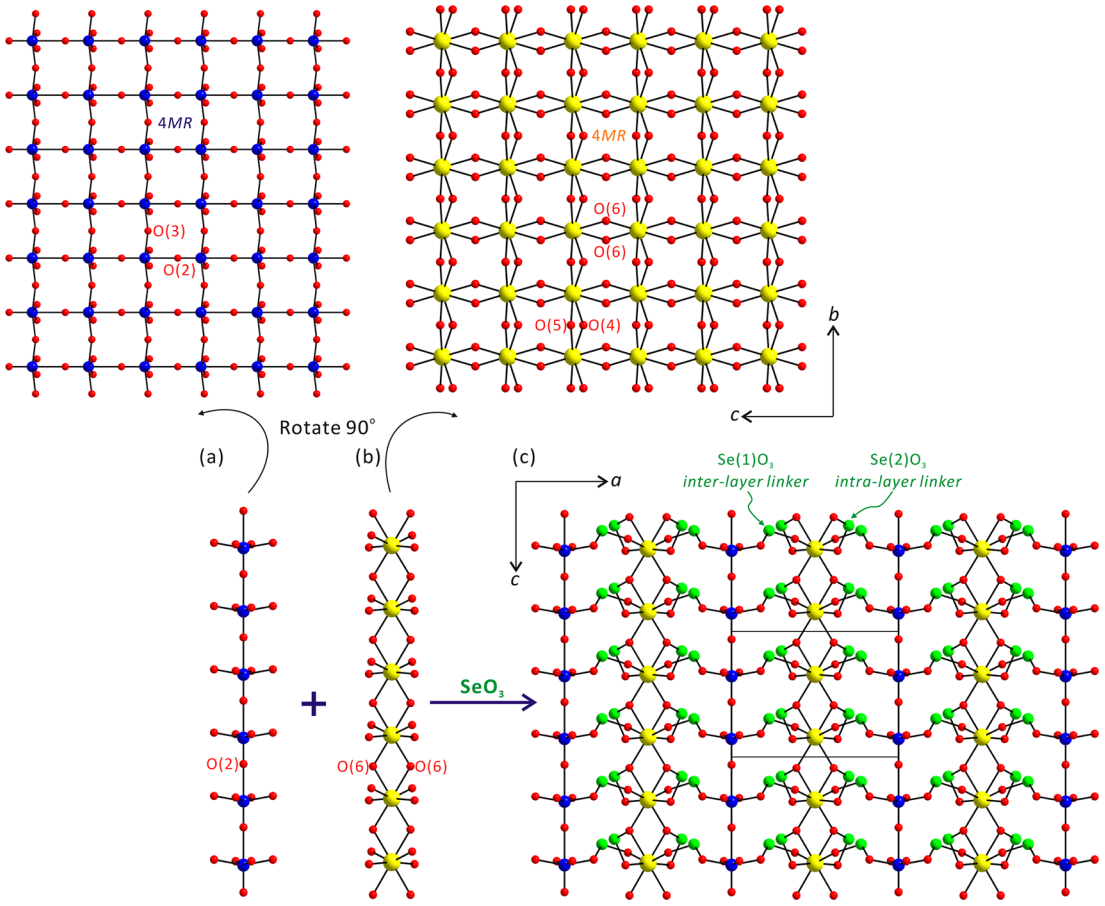

Figure 1. Ball-and-stick representations of (a) a layer of corner-shared VO_6 octahedra, (b) a layer of edge-shared YO_8 polyhedra, and (c) a completed three-dimensional framework for $YVSe_2O_8$ (blue, V; green, Se; yellow, Y; red, O). Note the $Se(1)O_3$ groups serve as an interlayer linker, and the $Se(2)O_3$ groups work as an interlayer linker.

TDS1032) was used. A detailed description of the methodology and the equipment used has been published.[15]

RESULTS AND DISCUSSION

Structures. $YVSe_2O_8$. A new quaternary mixed metal selenite material, $YVSe_2O_8$, crystallizes in the orthorhombic polar noncentrosymmetric space group, *Abm*2 (No. 39). The structural backbone of $YVSe_2O_8$ is composed of YO_8, VO_6, and SeO_3 polyhedra. The unique V^{5+} cation is in a severely distorted octahedral coordination environment with six oxygen atoms due to the SOJT distortion: the V^{5+} cation distorts toward a corner (local C_4 [001] direction) of the octahedron and results in one short [1.616(14) Å], four medium [1.923(9)−1.972(4) Å], and one long [2.301(14) Å] V−O bond distances. Two unique Se^{4+} cations exist within an asymmetric unit, in which both Se^{4+} cations contain the stereoactive lone pairs and exhibit asymmetric coordination environments. The Se−O bond distances range from 1.690(12) to 1.724(12) Å. The Y^{3+} cation is linked by eight oxygen atoms in distorted square antiprismatic coordination environment with Y−O bond lengths ranging from 2.326(9) to 2.369(9) Å. As seen in Figure 1a, the distorted VO_6 octahedra share their corners through O(2) and O(3) along the [001] and [010] directions, respectively. Thus, layers of corner-shared VO_6 octahedra are obtained in the *bc*-plane. Within the layer, four-membered rings (4MRs) are observed. The distorted YO_8 square antiprisms share their edges through O(6) along the [001] direction, and O(4) and O(5) along the [010] direction, which form other layers of edge-shared YO_8 polyhedra and their 4MRs in the *bc*-plane (see Figure 1b). Finally, the SeO_3 groups serve to link these VO_6 and YO_8 polyhedra. The $Se(1)O_3$ groups serve as an interlayer linker, whereas the $Se(2)O_3$ groups work as an interlayer connector (see Figure 1c). Thus, a three-dimensional framework structure of $YVSe_2O_8$ is completed. In connectivity terms, the structure of $YVSe_2O_8$ may be written as a neutral framework of $\{[YO_{8/3}]^{-2.333}[VO_{6/2}]^{-1.000}[Se(1)O_{2/2}O_{1/3}]^{+1.333}[Se(2)O_{3/3}]^{+2.000}\}^0$. Bond valence sum calculations[16] for the Y^{3+}, V^{5+}, and Se^{4+} result in values of 3.18, 4.62, and 3.89−3.91, respectively.

$YVTe_2O_8$. Another new mixed metal oxide, $YVTe_2O_8$ crystallizes in the monoclinic centrosymmetric space group *C*2/*m* (No. 12). $YVTe_2O_8$ is a three-dimensional quaternary Y^{3+}−V^{5+}−Te^{4+}−oxide containing distorted YO_8 polyhedra, VO_6 octahedra, and asymmetric TeO_3 groups. Within an asymmetric unit, a unique V^{5+} cation exists in a distorted octahedral coordination environment with six oxygen atoms. Similar to $YVSe_2O_8$, the unique V^{5+} cation distorts along the local C_4 direction and results in a short [1.628(4) Å], four intermediate [1.909(4)−1.953(2) Å], and a long [2.342(4) Å] V−O bond lengths. Four unique Te^{4+} cations are also in asymmetric trigonal pyramidal coordination environments with three oxygen atoms attributed to the lone pairs with Te−O bond distances ranging 1.846(5)−1.912(4) Å. There are two unique Y^{3+} cations that are surrounded by eight oxygen atoms

dx.doi.org/10.1021/ic402929m | *Inorg. Chem.* 2014, 53, 1250−1256

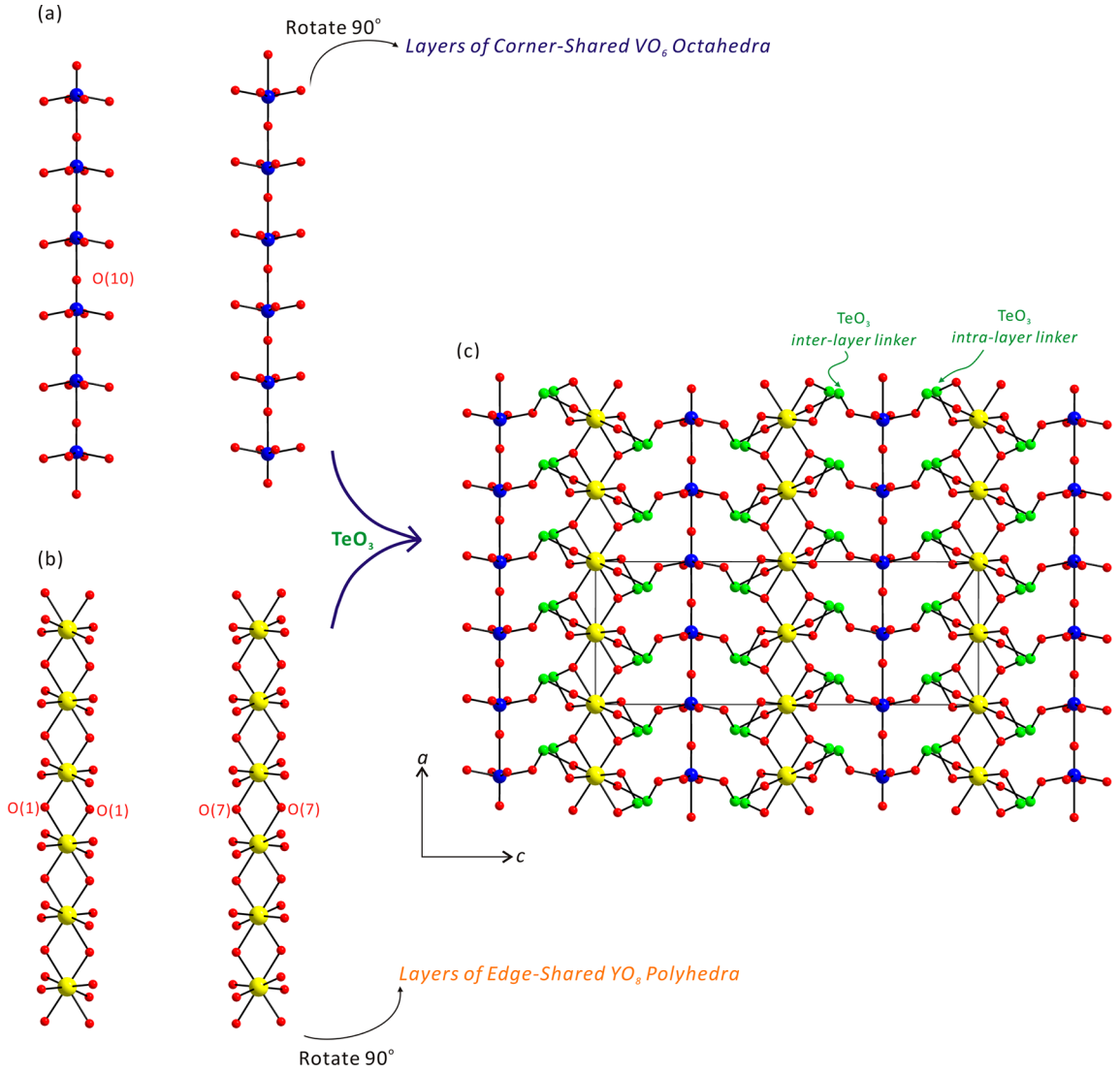

Figure 2. Ball-and-stick representations of (a) layers of corner-shared VO_6 octahedra, (b) layers of edge-shared YO_8 polyhedra, and (c) a completed three-dimensional framework for $YVTe_2O_8$ (blue, V; green, Te; yellow, Y; red, O). The lone pair polarizations associated with Te^{4+} cancel when taken as a whole.

in distorted square antiprismatic environments with Y−O bond lengths ranging from 2.304(3) to 2.439(4) Å.

The distorted VO_6 octahedra share their vertices through O(10) along the [100] direction, and O(9) and O(11) along the [010] direction, which generates layers of corner-shared VO_6 octahedra in the *ab*-plane (see Figure 2a). It should be noted that the short and the long V−O bonds alternate layer by layer along the [100] direction in $YVTe_2O_8$ (see Figure 2a). In NCS polar $YVSe_2O_8$, however, all of the short V−O bonds point toward the [001] direction, whereas all of the long V−O bonds orient toward the [00−1] direction (see Figure 1). Similar to those of $YVSe_2O_8$, other kinds of layers are also obtained by edge-sharing of the distorted YO_8 groups through O(1) [or O(7)] along the [100] direction, and O(2) and O(3) [or O(5) and O(8)] along the [010] direction (see Figure 2b). The TeO_3 groups serve as intra- and interlayer linkers and complete a three-dimensional framework structure of $YVTe_2O_8$ (see Figure 1c). One can easily notice that the lone pair on Te^{4+} points in approximately one of four directions, [001], [00−1], [−100], and [100] (see Figure 2c). Once taken as a whole, the lone pair polarizations concomitant with Te^{4+} cancel. In connectivity terms, the structure of $YVTe_2O_8$ can be described as a neutral framework of $\{[Y(1)O_{8/3}]^{-2.333}[Y(2)O_{8/3}]^{-2.333}2[VO_{6/2}]^{-1.000}[Te(1)O_{3/3}]^{+2.000}[Te(2)O_{2/2}O_{1/3}]^{+1.333}[Te(3)O_{2/2}O_{1/3}]^{+1.333}[Te(4)O_{3/3}]^{+2.000}\}^0$. Bond valence sum calculations[16] for the Y^{3+}, V^{5+}, and Te^{4+} result in values in the ranges 3.09−3.12, 4.68, and 3.80−3.88, respectively.

Infrared Spectroscopy. The infrared spectra of the reported materials reveal Y−O, V−O, Se−O, and Te−O vibrations. The Y−O vibrations are observed at ca. 406−487 cm^{-1}. The bands observed around 507−555 and 821−862 cm^{-1} can be assigned to O−V−O and V−O vibrations, respectively. The peaks occurring about 663−779 and 603−759 cm^{-1} may be attributable to Se−O and Te−O vibrations, respectively. The assignments agree well with those previously reported.[1h,7b,17] The infrared spectra have been included in the Supporting Information.

UV−Vis Diffuse Reflectance Spectroscopy. The UV−vis diffuse reflectance spectra for $YVSe_2O_8$ and $YVTe_2O_8$ have been obtained. Absorption (K/S) data were calculated from the Kubelka−Munk function:[13]

dx.doi.org/10.1021/ic402929m | Inorg. Chem. 2014, 53, 1250−1256

$$F(R) = \frac{(1-R)^2}{2R} = \frac{K}{S}$$

Here, K is the absorption, S the scattering, and R the reflectance. In the (K/S)-versus-E plots, extrapolating the linear part of the ascending curve to zero yielded the onset of absorption at 2.7 and 2.2 eV for $YVSe_2O_8$ and $YVTe_2O_8$, respectively. The band gaps for the reported materials may be due to the degree of V (3d) orbitals involved in the conduction bands, as well as the distortions originating from SeO_3 or TeO_3 polyhedra. The onsets of absorption values for the reported compounds are in good agreement with the previous studies of vanadium selenites and tellurites.[18] The (K/S)-versus-E plots for $YVSe_2O_8$ and $YVTe_2O_8$ have been included in the Supporting Information.

Thermogravimetric Analysis. The thermal characteristics of $YVSe_2O_8$ and $YVTe_2O_8$ were examined using thermogravimetric analysis. $YVSe_2O_8$ is thermally stable up to 500 °C. Above this temperature, the material breaks down to YVO_4[19] attributed to the sublimation of SeO_2, which was confirmed by powder XRD. With $YVTe_2O_8$, no weight loss was observed up to 1000 °C from the TGA. However, powder XRD measurements on $YVTe_2O_8$ at different temperatures reveal that the material decomposes to YVO_4[19] and $Y_2Te_6O_{15}$[20] at 750 °C. An endothermic peak occurring at the same temperature in the heating curve of the differential thermal analysis (DTA) diagram for $YVTe_2O_8$ is consistent with the variable temperature XRD data. The TG-DTA plots and XRD patterns for calcined products are found in the Supporting Information.

Powder Second-Harmonic Generation (SHG) Properties Measurements. $YVSe_2O_8$ crystallized in a noncentrosymmetric space group, *Abm*2; thus, its nonlinear optical (NLO) properties were investigated. Powder SHG measurements, using 1064 nm radiation, revealed that $YVSe_2O_8$ possessed a similar SHG efficiency to that of $NH_4H_2PO_4$ (ADP). The type 1 phase-matching capabilities of the material could be determined by sieving ground $YVSe_2O_8$ into several distinct particle sizes, ranging over 20−250 μm, and measuring the SHG as a function of particle size. As seen in Figure 3,

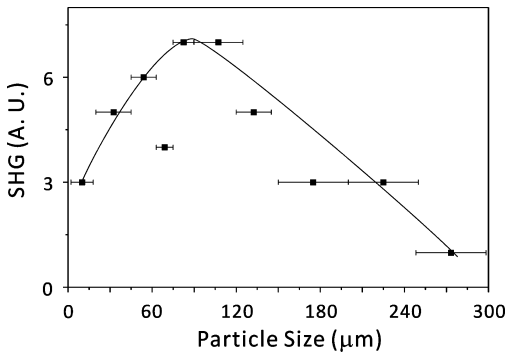

Figure 3. Type 1 phase matching curve for $YVSe_2O_6$. The curve is to guide the eye and is not a fit to the data.

$YVSe_2O_8$ turned out to be non-phase-matchable and could be classified as a class C SHG material, as defined by Kurtz and Perry.[14] If both of the SHG efficiency and the type 1 phase-matching capability of a material are disclosed, the bulk SHG efficiency, $\langle d_{eff}\rangle_{exp}$, can be estimated.[21] For $YVSe_2O_8$, $\langle d_{eff}\rangle_{exp}$ is calculated to be approximately 1.7 pm V^{-1}.

Structure−Property Relationships. The macroscopic NCS of $YVSe_2O_8$ can be analyzed by the alignment of the local asymmetric polyhedra. Furthermore, the observed SHG response and its origin may be explained by determining the net direction of the polarizations. The Y^{3+} is not a second-order Jahn−Teller distortive cation; thus, the effect toward the SHG efficiency arising from the distortion of YO_8 polyhedra would be negligible. The distorted VO_6 octahedra composed of the d^0 cation, V^{5+}, are aligned in one direction: the long and short V−O bonds alternate along the corner-shared chains, and a net moment is observed toward the [00−1] direction (see Figure 4). Finally, a net dipole moment can be expected from the

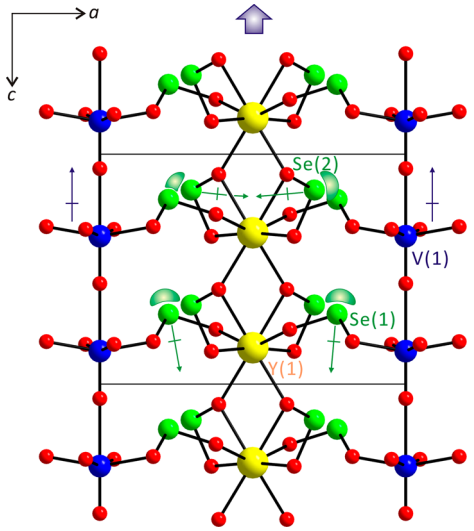

Figure 4. Ball-and-stick model of $YVSe_2O_6$ (blue, V; green, Se; yellow, Y; red, O). A moment is observed toward the [00−1] direction due to the alignment of the VO_6 octahedra with the C_4 out-of-center distortion. Another net moment occurs in the [001] direction attributed to the asymmetric $Se(1)O_3$ groups parallel toward the [00−1] direction. When taken as a whole considering the dipole moment calculations, a net moment is observed along the [00−1] direction.

alignment of asymmetric SeO_3 polyhedra containing lone pairs. As described before, there are two unique Se^{4+} cations within the asymmetric unit. For $Se(1)^{4+}$, the lone pairs point approximately parallel toward the [00−1] direction, and a moment occurs in the [001] direction (see Figure 4). However, the lone pairs on $Se(2)O_3^{4+}$ approximately point toward the [100] and [−100] directions, and the polarization almost cancels. Thus, a net moment occurring from SeO_3^{4+} polyhedra is expected in the [001] direction (see Figure 4). We found that the moments arising from VO_6 octahedra and SeO_3 polyhedra are in opposite directions. To decide a net direction as well as a net moment observed in $YVSe_2O_8$, local dipole moments for V^{5+} and Se^{4+} were calculated using the method described earlier.[22] By doing so, the local dipole moments for VO_6, $Se(1)O_3$, and $Se(2)O_3$ polyhedra in $YVSe_2O_8$ are calculated to be about 8.70, 7.83, and 9.42 D (Debyes), respectively. Taking the moments as a whole, a small net moment occurs along the [00−1] direction, which is consistent with our SHG measurements (similar to that of ADP). Also, it should be mentioned that the second-harmonic generating light (532 nm) may be underestimated attributed to the color of $YVSe_2O_8$. For comparison, local dipole moments for the VO_6 octahedron and two unique TeO_3 polyhedra, $Te(1)O_3$ and $Te(2)O_3$, in

dx.doi.org/10.1021/ic402929m | Inorg. Chem. 2014, 53, 1250−1256

centrosymmetric $YVTe_2O_8$ are also calculated, and they turn out to be quite similar values to those of $YVSe_2O_8$ and recently reported mixed metal oxides.[6e−g,7d,23] The calculated local dipole moments for the VO_6, SeO_3, and TeO_3 groups are summarized in Table 3.

Table 3. Calculation of Dipole Moments for VO_6, SeO_3, and TeO_3 Polyhedra (D = Debyes)

compound	species	dipole moment (D)
$YVSe_2O_8$	$V(1)O_6$	8.70
	$Se(1)O_3$	7.83
	$Se(2)O_3$	9.42
$YVTe_2O_8$	$V(1)O_6$	10.42
	$Te(1)O_3$	10.61
	$Te(2)O_3$	9.69

Although the centricities are different, both $YVSe_2O_8$ and $YVTe_2O_8$ contain VO_6 octahedra with the C_4 out-of-center distortion. Thus, it is worth quantifying the magnitude of out-of-center distortions (Δ_d) for VO_6 octahedra. Using the method used before,[3b] Δ_d values for VO_6 octahedra in $YVSe_2O_8$ and $YVTe_2O_8$ are calculated to be 0.69 and 0.72, respectively. The values are smaller than the average magnitude of the intraoctahedral distortion scale for V^{5+} (1.10).

Although stoichiometrically similar, $YVSe_2O_8$ crystallizes in the NCS space group and $YVTe_2O_8$ is CS. Since the average radii and the cation−lone pair distance for Te^{4+} are much greater than those for Se^{4+},[22a,24] $YVTe_2O_8$ requires more space around YO_8 polyhedra. In other words, if the larger TeO_3 polyhedra are aligned in the same direction within a limited space, unfavorable lone pair−lone pair interactions could be expected. Thus, the TeO_3 linkers align in opposite directions and result in CS space group (see Figure 2c). However, the smaller rigid SeO_3 groups could reside in a confined space without any repulsion and stabilize the NCS structure.

CONCLUSIONS

Single crystals and bulk polycrystalline samples of two new quaternary vanadium selenite and tellurite, i.e., $YVSe_2O_8$ and $YVTe_2O_8$, have been successfully synthesized. Crystallographic analyses indicate that both of the materials reveal three-dimensional framework structures that are composed of YO_8, VO_6, and SeO_3 or TeO_3 polyhedra with asymmetric coordination environments. While $YVSe_2O_8$ crystallizes in the orthorhombic polar NCS space group, *Abm*2, $YVTe_2O_8$ crystallizes in the monoclinic CS space group, *C*2/*m*. $YVSe_2O_8$ and $YVTe_2O_8$ are thermally stable up to 550 and 700 °C, respectively. Powder NLO measurements on NCS $YVSe_2O_8$ using 1064 nm radiation reveal that the compound is not phase-matchable (type 1) with a SHG efficiency similar to that of ADP. Dipole moment calculations explain that the SHG efficiency is consistent with a small net moment arising from the alignments of VO_6 octahedra and asymmetric SeO_3 groups.

ASSOCIATED CONTENT

Supporting Information

X-ray crystallographic file in CIF format, calculated and observed X-ray diffraction patterns, infrared spectra, UV−vis diffuse reflectance spectra, and thermogravimetric analysis diagrams for $YVSe_2O_8$ and $YVTe_2O_8$. This material is available free of charge via the Internet at http://pubs.acs.org.

AUTHOR INFORMATION

Corresponding Author

*E-mail: kmok@cau.ac.kr. Phone: +82-2-820-5197. Fax: +82-2-825-4736.

Notes

The authors declare no competing financial interest.

ACKNOWLEDGMENTS

This research was supported by Basic Science Research Program through the National Research Foundation of Korea (NRF) funded by Ministry of Education, Science & Technology (Grant 2013R1A2A2A01007170).

REFERENCES

(1) (a) Nye, J. F. *Physical Properties of Crystals*; Oxford University Press: Oxford, U.K., 1957. (b) Jona, F.; Shirane, G. *Ferroelectric Crystals*; Pergamon Press: Oxford, 1962. (c) Cady, W. G. *Piezoelectricity; An Introduction to the Theory and Applications of Electromechanical Phenomena in Crystals*; Dover: New York, 1964. (d) Lang, S. B. *Sourcebook of Pyroelectricity*; Gordon & Breach Science: London, 1974. (e) Ok, K. M.; Bhuvanesh, N. S. P.; Halasyamani, P. S. *Inorg. Chem.* **2001**, *40*, 1978−1980. (f) Ok, K. M.; Halasyamani, P. S. *Angew. Chem., Int. Ed.* **2004**, *43*, 5489−5491. (g) Kim, J.-H.; Baek, J.; Halasyamani, P. S. *Chem. Mater.* **2007**, *19*, 5637−5641. (h) Kim, M. K.; Kim, S.-H.; Chang, H.-Y.; Halasyamani, P. S.; Ok, K. M. *Inorg. Chem.* **2010**, *49*, 7028−7034. (i) Nguyen, S. D.; Yeon, J.; Kim, S.-H.; Halasyamani, P. S. *J. Am. Chem. Soc.* **2011**, *133*, 12422−12425. (j) Nguyen, S. D.; Halasyamani, P. S. *Inorg. Chem.* **2013**, *52*, 2637−2647.

(2) (a) Opik, U.; Pryce, M. H. L. *Proc. R. Soc. London* **1957**, *A238*, 425−447. (b) Bader, R. F. W. *Can. J. Chem.* **1962**, *40*, 1164−1175. (c) Pearson, R. G. *J. Am. Chem. Soc.* **1969**, *91*, 4947−4955. (d) Pearson, R. G. *THEOCHEM* **1983**, *103*, 25−34. (e) Wheeler, R. A.; Whangbo, M.-H.; Hughbanks, T.; Hoffmann, R.; Burdett, J. K.; Albright, T. A. *J. Am. Chem. Soc.* **1986**, *108*, 2222−2236. (f) Kunz, M.; Brown, I. D. *J. Solid State Chem.* **1995**, *115*, 395−406. (g) Oh, S.-J.; Lee, D. W.; Ok, K. M. *Dalton Trans.* **2012**, *41*, 2995−3000.

(3) (a) Halasyamani, P. S.; Poeppelmeier, K. R. *Chem. Mater.* **1998**, *10*, 2753−2769. (b) Halasyamani, P. S. *Chem. Mater.* **2004**, *16*, 3586−3592.

(4) (a) Lefebvre, I.; Lannoo, M.; Allan, G.; Ibanez, A.; Fourcade, J.; Jumas, J. C. *Phys. Rev. Lett.* **1987**, *59*, 2471−2474. (b) Lefebvre, I.; Szymanski, M. A.; Olivier-Fourcade, J.; Jumas, J. C. *Phys. Rev. B* **1998**, *58*, 1896−1906. (c) Watson, G. W.; Parker, S. C. *J. Phys. Chem. B* **1999**, *103*, 1258−1262. (d) Watson, G. W.; Parker, S. C.; Kresse, G. *Phys. Rev. B* **1999**, *59*, 8481−8486. (e) Seshadri, R.; Hill, N. A. *Chem. Mater.* **2001**, *13*, 2892−2899. (f) Waghmare, U. V.; Spaldin, N. A.; Kandpal, H. C.; Seshadri, R. *Phys. Rev. B* **2003**, *67*, 125111/1−125111/10. (g) Walsh, A.; Payne, D. J.; Egdell, R. G.; Watson, G. W. *Chem. Soc. Rev.* **2011**, *40*, 4455−4463.

(5) (a) Wu, Y. C.; Sasaki, T.; Nakai, S.; Yokotani, A.; Tang, H. G.; Chen, C. T. *Appl. Phys. Lett.* **1993**, *62*, 2614−2615. (b) Chen, C. T.; Ye, N.; Lin, J.; Jiang, J.; Zeng, W. R.; Wu, B. C. *Adv. Mater.* **1999**, *11*, 1071−1078. (c) Pan, S.; Smit, J. P.; Watkins, B.; Marvel, M. R.; Stern, C. L.; Poeppelmeier, K. R. *J. Am. Chem. Soc.* **2006**, *128*, 11631−11634. (d) Inaguma, Y.; Yoshida, M.; Katsumata, T. *J. Am. Chem. Soc.* **2008**, *130*, 6704−6705. (e) Jiang, H.; Kong, F.; Fan, Y.; Mao, J.-G. *Inorg. Chem.* **2008**, *47*, 7430−7437. (f) Zhang, D.; Johnsson, M. *Acta Crystallogr., Sect. E* **2008**, *64*, i26/1−i26/6. (g) Wu, H. P.; Pan, S. L.; Poeppelmeier, K. R.; Li, H. Y.; Jia, D. Z.; Chen, Z. H.; Fan, X. Y.; Yang, Y.; Rondinelli, J. M.; Luo, H. S. *J. Am. Chem. Soc.* **2011**, *133*, 7786−7790. (h) Yu, H. W.; Wu, H. P.; Pan, S. L.; Yang, Z. H.; Su, X.; Zhang, F. F. *J. Mater. Chem.* **2012**, *22*, 9665−9670.

(6) (a) Sykora, R. E.; Ok, K. M.; Halasyamani, P. S.; Albrecht-Schmitt, T. E. *J. Am .Chem. Soc.* **2002**, *124*, 1951−1975. (b) Goodey, J.; Ok, K. M.; Broussard, J.; Hofmann, C.; Escobedo, F. V.; Halasyamani, P. S. *J. Solid State Chem.* **2003**, *175*, 3−12. (c) Ok, K.

M.; Baek, J.; Halasyamani, P. S.; O'Hare, D. *Inorg. Chem.* **2006**, *45*, 10207−10214. (d) Choi, M.-H.; Kim, S.-H.; Chang, H. Y.; Halasyamani, P. S.; Ok, K. M. *Inorg. Chem.* **2009**, *48*, 8376−8382. (e) Lee, D. W.; Bak, D.-b.; Kim, S. B.; Kim, J.; Ok, K. M. *Inorg. Chem.* **2012**, *51*, 7844−7850. (f) Oh, S.-J.; Lee, D. W.; Ok, K. M. *Inorg. Chem.* **2012**, *51*, 5393−5399. (g) Lee, D. W.; Ok, K. M. *Inorg. Chem.* **2013**, *52*, 5176−5184.

(7) (a) Li, P. X.; Kong, F.; Hu, C. L.; Zhao, N.; Mao, J.-G. *Inorg. Chem.* **2010**, *49*, 5943−5952. (b) Li, P.-X.; Zhang, S.-Y.; Mao, J.-G. *Dalton Trans.* **2010**, *39*, 11560−11567. (c) Lee, D. W.; Oh, S. J.; Halasyamani, P. S.; Ok, K. M. *Inorg. Chem.* **2011**, *50*, 4473−4480. (d) Kim, Y. H.; Lee, D. W.; Ok, K. M. *Inorg. Chem.* **2013**, *52*, 11450−11456.

(8) Harrison, W. T. A. *Acta Crystallogr., Sect. E* **2006**, *62*, i152−i154.

(9) *SAINT, Program for Area Detector Absorption Correction, version 4.05*; Siemens Analytical X-ray Instruments: Madison, WI, 1995.

(10) Sheldrick, G. M. *SHELXS-97—A Program for Automatic Solution of Crystal Structures*; University of Göttingen: Göttingen, Germany, 1997.

(11) Sheldrick, G. M. *SHELXL-97—A Program for Crystal Structure Refinement*; University of Göttingen: Göttingen, Germany, 1997.

(12) Farrugia, L. J. *J. Appl. Crystallogr.* **1999**, *32*, 837−838.

(13) (a) Kubelka, P.; Munk, F. *Z. Tech. Phys.* **1931**, *12*, 593. (b) Tauc, J. *Mater. Res. Bull.* **1970**, *5*, 721−729.

(14) Kurtz, S. K.; Perry, T. T. *J. Appl. Phys.* **1968**, *39*, 3798−3813.

(15) Ok, K. M.; Chi, E. O.; Halasyamani, P. S. *Chem. Soc. Rev.* **2006**, *35*, 710−717.

(16) (a) Brown, I. D.; Altermatt, D. *Acta Crystallogr., Sect. B* **1985**, *41*, 244−247. (b) Brese, N. E.; O'Keeffe, M. *Acta Crystallogr., Sect. B* **1991**, *B47*, 192−197.

(17) Raju, K. V.; Raju, C. N.; Sailaja, S.; Dhoble, S. J.; Reddy, B. S. *J. Lumin.* **2013**, *134*, 297−302.

(18) (a) Sivakumar, T.; Ok, K. M.; Halasyamani, P. S. *Inorg. Chem.* **2006**, *45*, 3602−3605. (b) Chang, H. Y.; Kim, S.-H.; Ok, K. M.; Halasyamani, P. S. *Chem. Mater.* **2009**, *21*, 1654−1662.

(19) Chakoumakos, B. C.; Abraham, M. M.; Boatner, L. A. *J. Solid State Chem.* **1994**, *109*, 197−202.

(20) Noguera, O.; Jouin, J.; Masson, O.; Jancar, B.; Thomas, P. *J. Eur. Ceram. Soc.* **2012**, *32*, 4263−4269.

(21) Goodey, J.; Broussard, J.; Halasyamani, P. S. *Chem. Mater.* **2002**, *14*, 3174−3180.

(22) (a) Galy, J.; Meunier, G. *J. Solid State Chem.* **1975**, *13*, 142−159. (b) Maggard, P. A.; Nault, T. S.; Stern, C. L.; Poeppelmeier, K. R. *J. Solid State Chem.* **2003**, *175*, 27−33. (c) Izumi, H. K.; Kirsch, J. E.; Stern, C. L.; Poeppelmeier, K. R. *Inorg. Chem.* **2005**, *44*, 884−895.

(23) (a) Kim, M. K.; Jo, V.; Lee, D. W.; Ok, K. M. *Dalton Trans.* **2010**, *39*, 6037−6042. (b) Lee, D. W.; Ok, K. M. *Solid State Sci.* **2010**, *12*, 2036−2041. (c) Lee, D. W.; Kim, S. B.; Ok, K. M. *Inorg. Chem.* **2012**, *51*, 8530−8537.

(24) Shannon, R. D. *Acta Crystallogr., Sect. A* **1976**, *32*, 751−767.